

Non-destructive inspection & sub-wavelength characterization

Robert Malkin¹

¹Ultrasonics and Non Destructive Testing, Mechanical Engineering, Queens School of Engineering, University of Bristol, Bristol, United Kingdom

Phased array transducers have in recent years allowed for ever increasing imaging capabilities in the field of non-destructive inspection. By capturing the maximum possible amount of acoustic information we are able to utilize imaging algorithms which bring unparalleled resolution and flexibility to industrial inspections. This talk will cover the background of acoustic array imaging and detail current trends and ongoing challenges being addressed at the University of Bristol.

Keywords: total focusing method, phased array transducer, ultrasonic, sub-wavelength imaging, defect characterization,

1. Introduction

Collectively the terms non-destructive inspection (NDI), non-destructive testing (NDT) and non-destructive evaluation (NDE) cover a range of analysis techniques to assess the properties of a material/structure without causing damage. They play a central role in inspections of safety critical structures in areas such as aerospace, nuclear engineering and the oil & gas industries. Common methods include; visual inspections (economical, safe and rapid but limited to surfaces only), dye penetrant (economical and minimally invasive but limited to surface breaking defects), x-ray (inspects whole structure at high resolution but dangerous, slow and size limited), eddy current (high resolution but offers relatively shallow surface penetration) and ultrasonic testing (safe, deep sample penetration but can be limited by acoustic scattering and physical access).

Ultrasonic testing was first utilized in 1931 to locate flaws in solid metal sheets. Since then it has become an advanced inspection technique amenable to a range of materials, including numerous applications in medicine. Here we present an overview of the acoustic NDT imaging research conducted at the University of Bristol.

2. Array imaging

The current 'gold standard' array imaging technique, developed at Bristol, is the total focusing method (TFM). It allows for unprecedented imaging resolution and flexibility. TFM relies on acquiring the maximum amount of acoustic information possible and then applying post-capture processing for imaging. It is best described in two stages, the data acquisition and the TFM algorithm.

2.1 Phased array transducer

In recent years phased array transducers have become more sophisticated and affordable. Traditionally they come in linear, annular or 2D array types with element numbers from 16 to 256. The most common inspection materials in engineering are metallic and given their finite grain sizes (which result in scattering and signal degradation) the acoustic frequencies used are usually between 2-20MHz. For flat surfaces, arrays can be used

in direct contact (with coupling gel applied at the interface) or for complex geometries they may be used in immersion where water couples the acoustic wave from the array to the material/structure under inspection.

2.2 Full matrix capture

TFM relies on acquiring all the possible acoustic information for a phased array [1]. This is done by transmitting an acoustic pulse on a single element and receiving the time-domain data on all others. This is done sequentially for all elements in the array (this places some limits on using TFM for non-stationary objects). For an array with n elements this results in n^2 measurements. The transmitting, receiving and digitizing of the acquired data is usually performed with an array controller, see Figure 1.



Figure 1: A commercial phased array controller, phased array, metal sample and imaging software. (Image courtesy of MicroPulse USA.)

2.3 Total focusing method

In TFM we first define an imaging area of interest within close proximity to the array, shown in Figure 2. Within this region we generate a grid of imaging pixels.

The intensity of the image at each point is given by $I(x,z)$ as shown in Eq 1.

$$I(x, z) = \left| \sum h_{t_x, r_x} \left(\frac{\sqrt{(x_{t_x} - x_{ref})^2 + z_{ref}^2} + \sqrt{(x_{r_x} - x_{ref})^2 + z_{ref}^2}}{c} \right) \right| \quad (1)$$

Where h is Hilbert transform of the time domain signal and c the wave speed.

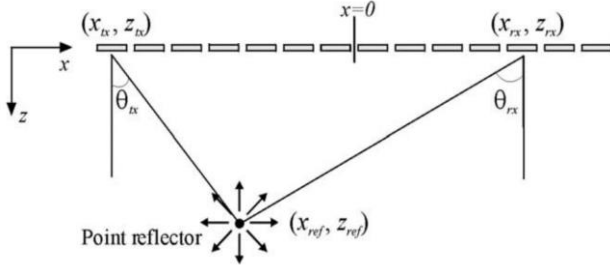


Figure 2: Imaging area of interest below a transducer. Here we show 14 elements (where subscript t_x and r_x are transmit and receive elements respectively) of a transducer and a single point in the TFM image (at x_{ref}, z_{ref}).

An example TFM image is shown in Figure 3.

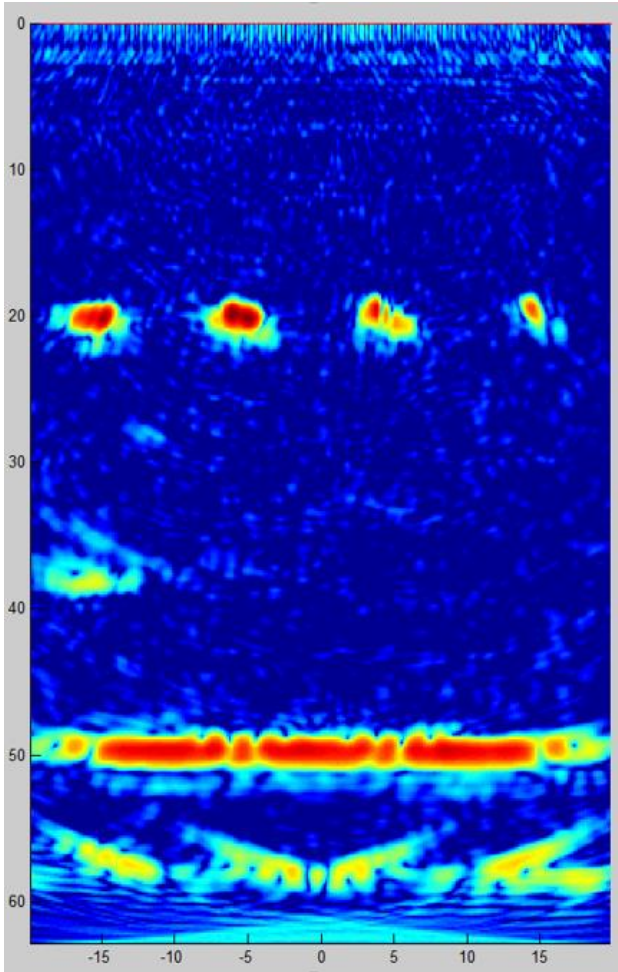


Figure 3: TFM image of stainless steel test specimen. Image shows 4 defects at 20mm depth and the back face of the specimen at 50mm.

2.4 Complex geometries

For inspections where the surfaces of the material/structure are not suitable for direct contact with the probe, immersion imaging is undertaken. To compensate for the combination of water between the array elements and surface, and a non-flat surface, the TFM imaging algorithm is modified using delay laws and ray tracing. This added complexity increases the computational resources needed for imaging (although this is becoming

less of an issue).

3D volumetric imaging using TFM is also possible using a 2D array type transducer. Computational resources for 3D imaging are however significantly higher given the additional dimension for a 3D image.

3. Sub-wavelength characterization

For safety critical systems where a defect is identified there is a worst-case scenario approach to assessing the severity of the defect. This will often result in structures with benign defects being taken out of service needlessly. This has been a key driver in our work to accurately characterize a defect.

The image shown in Figure 3 shows 4 approximately circular defects. In reality these defects are 4 flat slots 1mm in length at 4 different rotations (i.e. $- / /$). At 5MHz in stainless steel the wavelength is ≈ 1.2 mm (while higher frequencies would theoretically yield increased resolution they also result in greater scattering which limits imaging resolution). Using TFM our resolution is approximately equal to that of 1-2 wavelengths.

Characterizing a defect smaller than a wavelength can be performed by examining the scattering matrix of a defect.

3.1 S-matrix

The scattering matrix, or S-matrix, describes the amplitude and phase of the scattered field of a defect in the far field, and has been shown to encode the far-field information arising from all wave-scatterer interactions [2]. Let \mathbf{r} be the position vector of a point in the x - z plane which in polar coordinates is given by, $\mathbf{r} = (r, \theta)$; here $r = |\mathbf{r}|$ and θ is measured from the positive z -axis. For 2-D problems, the far-field scattering amplitude is defined by Eq 2, [3].

$$u^{SC}(\mathbf{r}) = \sqrt{\frac{2}{\pi}} e^{-\frac{i\pi}{4}} \frac{e^{ikr}}{\sqrt{kr}} S(\theta) \quad (2)$$

Where $i^2 = -1$, $k = \omega/c_L$ and c_L is the longitudinal wave velocity. For a given angular frequency, ω , $S(\theta, \omega)$ gives the field scattered in the direction θ [4]. An example S matrix is shown in Figure 4.

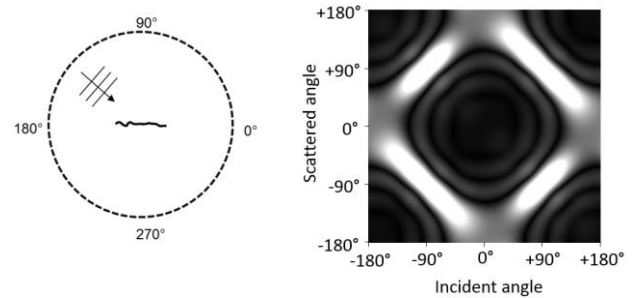


Figure 4: S-Matrix. Left: The S-matrix is defined as the far-field amplitude of a scattered plane wave (shown with an incidence angle of $\approx 135^\circ$) for all incidence angles. Right: Normalized scattering matrix of a defect (amplitude shown from 0-1). The S-matrix for a 2mm flat crack at 5MHz. Each S-matrix is singular and unique for a given defect.

3.2 Defect database

Given that each S-matrix maps uniquely to a single defect

geometry if we compare an experimentally acquired S-matrix, S_{EXP} , to a database of pre-calculated S-matrices, S_{CALC} , we should be able to characterize the defect (for a flat crack this would be its length and rotation). This relies on S_{EXP} being contained within our S_{CALC} database. To demonstrate this we compute a large number of S-matrices covering a limited type of defect: flat cracks from 0.2-2.0mm in length, at all rotations, at frequencies between 2-20MHz. Per frequency this gave us 5400 S_{CALC} entries in our database. S_{CALC} were computed using a highly efficient finite element approach [5].

3.3 Comparison of S-matrices

An important aspect of searching our database for a match between S_{CALC} and S_{EXP} is the comparison metric. We have used the structural similarity metric (SSIM) which gives a correlation (0 to 1) of the similarity between two datasets. The SSIM has been shown to be well suited to such an application [6].

When comparing the 4 S_{EXP} from Figure 3 to our database the SSIM correlation values were >0.97 . Low SSIM values would indicate that the real defect is not contained within our database.

3.4 Measurement certainty

The usual outcome of a database search will be a number of SSIM scores (the number being equal to the number of database entries). While choosing the maximum SSIM score tells us which pair of S_{EXP} & S_{CALC} are most similar it does not give us any information on the possible error tolerance of our comparison result. By exploring the information contained within an S-matrix and incorporating measurement noise we have proposed a method of measuring the error of our characterization, e.g. crack length 1.2 ± 0.2 mm, rotation $74 \pm 6^\circ$ (detailed in [4]).

3.5 General classification

In order to expand the classification capability of our database based approach we can ‘simplify’ the geometry of a defect using principle component analysis (PCA) and dynamic classifiers [7]. This approach allows us to classify the general nature of a defect with estimates of its shape/orientation without having to use an impractically large database, the approach also benefits from being inherently insensitive to noise as may be contained within an S_{EXP} . Recent results, shown in Figure 5, demonstrate that we can accurately estimate the shape of a defect. More accurate geometry estimates may be theoretically possible, but may not yield real world benefits.

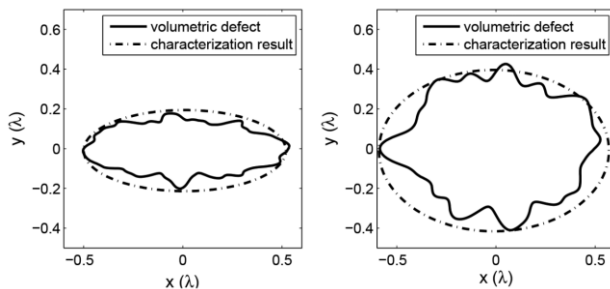


Figure 5: Accurate characterization of volumetric defects using a dynamic classifier approach.

4. Future work

With increasing computing power, phased array acoustic imaging systems are likely to become a ubiquitous part of inspection regimes. Phased array transducers are now offered in a range of types across a wide range of frequencies. The work of the Ultrasonics and Non Destructive Testing group at the University of Bristol will continue to develop imaging algorithms and characterization approaches to increase the capabilities of phased array transducers. Explorations into non-linear acoustic imaging are currently underway with promising initial results.

5. Summary

Non destructive inspections of materials/structures is a growing field of academic study and industrial utilisation. Advancements in computational techniques have allowed for the imaging of internal structures with unprecedented detail. Along with large defect databases and efficient searching algorithms we are able to locate a defect and classify its shape, which is vital for assessing its severity.

References

- [1] Holmes C, *et al.*: Post-processing of the full matrix of ultrasonic transmit–receive array data for non-destructive evaluation, *NDT&E*. 38 (2005), 701-711.
- [2] Achenbach JD: Quantitative nondestructive evaluation, *Int J Solids Struct*. 37 (2000), 13-27.
- [3] Martin PA: Multiple Scattering - interaction of time-harmonic waves with N obstacles. Cambridge University Press, Cambridge (2006).
- [4] Malkin R, *et al.*: A numerical database for ultrasonic defect characterisation using array data: Robustness and accuracy, *NDT&E*. 83 (2016), 94-103.
- [5] Velichko A, *et al.*: A generalized approach for efficient finite element modeling of elastodynamic scattering in two and three dimensions. *J Acoust Soc Am*. 128 (2010) 1004-14.
- [6] Bai L, *et al.*: Ultrasonic characterization of crack-like defects using scattering matrix similarity metrics. *IEEE Trans Ultrason Ferroelectr Freq Control* 62 (2015) 545–59.
- [7] Bai L, *et al.*: Characterization of Defects Using Ultrasonic Arrays: A Dynamic Classifier Approach. *IEEE Trans Ultrason Ferroelectr Freq Control* 62 (2015) 2146–60.

